HHS Public Access

Author manuscript

Nat Struct Mol Biol. Author manuscript; available in PMC 2016 May 18.

Published in final edited form as:

Nat Struct Mol Biol. 2015 December ; 22(12): 968–975. doi:10.1038/nsmb.3116.

Structural basis for catalytic activation by the human ZNF451 SUMO E3 ligase

Laurent Cappadocia[1], **Andrea Pichler**[2], and **Christopher D. Lima**[1,3]

[1]Structural Biology Program, Sloan Kettering Institute, New York, New York, USA

[2]Department of Epigenetics, Max Planck Institute of Immunobiology and Epigenetics, Freiburg, Germany

[3]Howard Hughes Medical Institute, Sloan Kettering Institute, New York, New York, USA

Abstract

E3 protein ligases enhance transfer of ubiquitin-like (Ubl) proteins from E2 conjugating enzymes to substrates by stabilizing the thioester-charged E2~Ubl in a closed configuration optimally aligned for nucleophilic attack. Here, we report biochemical and structural data that define the N-terminal domain of the *Homo sapiens* ZNF451 as the catalytic module for SUMO E3 ligase activity. ZNF451 catalytic module contains tandem SUMO interaction motifs (SIMs) bridged by a Proline-Leucine-Arginine-Proline (PLRP) motif. The first SIM and PLRP motif engage thioester charged E2~SUMO while the next SIM binds a second molecule of SUMO bound to the backside of E2. We show that ZNF451 is SUMO2 specific and that SUMO-modification of ZNF451 may contribute to activity by providing a second molecule of SUMO that interacts with E2. Our results are consistent with ZNF451 functioning as a *bona fide* SUMO E3 ligase.

Introduction

Ubiquitin (Ub) or ubiquitin-like (Ubl) proteins regulate numerous cellular processes (reviewed in ref. [1]) and are typically conjugated to lysine residues of substrate proteins by the sequential activities of an E1 activating enzyme, an E2 conjugating enzyme and E3 ligases that facilitate Ub or Ubl transfer from the charged E2 to target substrates (reviewed in ref. [2]). The SUMO pathway includes a single E1, a single E2 and several E3s. SUMO conjugation can occur in the absence of an E3 via E2 recognition of a Ψ-K-X-E substrate consensus motif where K is the target lysine and Ψ is a hydrophobic residue[3,4]. Three genes encode unique SUMO proteins in humans. SUMO2 and SUMO3 share 97% sequence identity in their mature form and include a N-terminal Ψ-K-X-E substrate consensus motif

Correspondence should be addressed to C.D.L. (; Email: limac@mskcc.org)

Accession codes

Coordinates and structure factors have been deposited in the Protein Data Bank under accession code 5D2M.

Author Contributions

A.P. initiated the project. L.C. and C.D.L designed experiments that L.C. performed. L.C. and C.D.L. wrote the manuscript with input from A.P.

that is used to form SUMO chains[5]. SUMO1 is present in cells at lower abundance[6], shares 50% sequence identity with SUMO2 and SUMO3 and does not efficiently form chains[5].

E3 ligases can decrease the binding constant for substrate while increasing the rate of transfer, thus resulting in an increase in the specificity constant (rate constant/binding constant). Mechanistically, E3 ligases stimulate Ub^D or Ubl^D~E2 thioester discharge (where ^{D} denotes the donor Ub or Ubl and "~" denotes a covalent bond) by positioning Ub^D or Ubl^D in a closed and active conformation primed for conjugation (reviewed in ref. [2]). This was first demonstrated for the SUMO E3 ligase RANBP2[7]. Subsequent analysis of the Ub~UBCH5–BRCA1–BARD1 complex by nuclear magnetic resonance suggested a closed conformation for Ub[8]. Several structures and biochemical characterization of ubiquitin and NEDD8 E3 ligases have also been reported wherein the Ub^D or Ubl^D~E2 is arranged in a similar closed configuration, albeit stabilized by interactions that are unique to the ubiquitin and NEDD8 RING E3 ligase systems[7,9–15]. This mechanism is also employed by Ub E2s that induce a closed configuration in the absence of E3[16,17].

A few *bona fide* SUMO E3 ligases have been identified. Siz and PIAS proteins belong to the SP-RING family of E3 ligases that utilize a RING domain to interact with the charged E2[18,19]. RANBP2 belongs to a second class of SUMO E3 ligase that coordinates the charged E2 using the IR1-M-IR2 motif[20] wherein each IR constitutes a catalytic module that includes a SUMO-Interacting Motif (SIM) that binds $SUMO^D$ in the context of thioester charged $SUMO^D$~E2 followed by additional structural elements that engage the interface between $SUMO^D$ and E2 before wrapping around the backside of the E2[7]. SIMs are short motifs typically composed of four hydrophobic residues succeeded or preceded by acidic residues that bind SUMO through β-strand complementation with SUMO's β-sheet in parallel or antiparallel orientation[7,21–23]. Other SUMO E3 ligases have been proposed however their mechanism of action remains elusive. Some of these, such as PC2 and SLX4, possess multiple SIMs and appear to stimulate SUMO-conjugation in a SIM-dependent manner[24–27].

In addition to interacting with $SUMO_D$, the SUMO E2 UBC9 can interact with a second molecule of SUMO through non-covalent interactions on the opposite surface or backside of E2 to form a E2–$SUMO^B$ complex[28–32] where ^{B} denotes interaction with the backside of the E2. E2–$SUMO^B$ interactions in the SUMO pathway are structurally analogous to that observed for E2–Ub^B complexes in the ubiquitin pathway as exemplified by UBCH5–Ub^B, RAD6–Ub^B and MMS2–Ub^B (refs. [33–35]). The UBCH5–Ub^B non-covalent interaction was shown to be important for increasing the rate of chain formation[33] and a similar role has been proposed for the UBC9–$SUMO^B$ interaction[30,32,35]. Although structurally similar, a notable difference between E2–Ub^B and E2–$SUMO^B$ interactions is that E2–$SUMO^B$ binding is estimated at ~100 nM affinity[29,32] while E2–Ub^B interaction occurs with affinities measured at >100 μM[10,33]. Recent work also suggests that E2–Ub^B interaction may stimulate Ub^D conjugation through an allosteric mechanism[10], however it remains unclear if this is true for E2–$SUMO^B$ interaction.

Several lines of evidence suggest that ZNF451 may constitute another class of SUMO E3 ligase. ZNF451 includes two predicted N-terminal SIMs followed by twelve C_2H_2 zinc

finger domains and a ubiquitin-interacting motif (Fig. 1a). ZNF451 interacts with SUMO and SUMO conjugating enzymes and it localizes to the PML nuclear bodies in a SUMO-dependent manner[36]. ZNF451 is targeted by SUMO-modification on multiple lysine residues[3,37–40] and ZNF451 modification was shown to occur *in vitro* in a SIM-dependent manner[36]. To understand if ZNF451 is a *bona fide* SUMO E3 Ligase, we performed structural and biochemical analyses and, along with along with Eisenhardt et al.[41], show that a N-terminal ZNF451 domain encompassing tandem SIMs and an intervening PLRP motif catalyzes SUMO E3 ligase activity with a preference for SUMO2. We establish that ZNF451 preferentially interacts with $SUMO^{D}$~E2–$SUMO^{B}$ in comparison to $SUMO^{D}$~E2 or E2–$SUMO^{B}$. The first SIM engages $SUMO^{D}$, the second SIM engages $SUMO^{B}$, and the intervening PLRP motif wedges into the interface between $SUMO^{D}$ and $SUMO^{B}$ to establish contacts to the E2. Similar to other E3 complexes, ZNF451 increases the rate of catalysis by coordinating thioester charged $SUMO^{D}$~E2 in an activated 'closed' configuration and it increases the binding affinity for substrates. We further show that SUMO modified ZNF451 can bypass the requirement for exogenous $SUMO^{B}$, presumably because SUMO modified ZNF451 provides the additional molecule of SUMO in *cis*.

Results

ZNF451 N-terminal domain catalyzes SUMO2 E3 ligase activity

To quantitatively assess if the N-terminal domain of ZNF451 displays SUMO E3 ligase activity *in vitro*, we monitored SUMO2 (Fig. 1b and Supplementary Table 1) and SUMO1 (Fig. 1c and Supplementary Table 1) conjugation to the model substrate p53 in absence or presence of a N-terminal domain of ZNF451 encompassing the two SIMs within residues 2–56. These assays, performed in single-turnover conditions, reveal that $ZNF451_{2–56}$ enhances conjugation to p53 with SUMO2 and SUMO1 by factors of 22 and 10, respectively, through a decrease in K_d and an increase in k_2. To explore if ZNF451 binds $SUMO^{D}$~E2–$SUMO^{B}$ better than $SUMO^{D}$~E2 we repeated assays in the presence of exogenous SUMO. $SUMO2_{15–89}$ and $SUMO1_{19–94}$ include the SUMO Ubl domain but lack the C-terminal di-glycine motif necessary for SUMO conjugation and, in the case of SUMO2, the canonical SUMO consensus acceptor necessary for chain formation[5]. In contrast to UBCH5–Ub^{B}, where non-covalent interaction modestly increased E2 efficiency in an E3-independent manner[10], addition of exogenous $SUMO1_{19–94}$ or $SUMO2_{15–89}$ in the absence of $ZNF451_{2–56}$ resulted in a decrease in SUMO conjugation to p53 by a factor of 2–3. Importantly, while exogenous $SUMO1_{19–94}$ increased $ZNF451_{2–56}$-dependent activity by a factor of 6, exogenous $SUMO2_{15–89}$ increased $ZNF451_{2–56}$-dependent activity with $SUMO2^{D}$ by a factor of 215, thus suggesting that $ZNF451_{2–56}$ possesses a stronger preference for $SUMO2^{D}$~E2–$SUMO2^{B}$ compared to $SUMO1^{D}$~E2–$SUMO1^{B}$. Furthermore, the increase in the specificity constant observed for $ZNF451_{2–56}$ with SUMO2 is comparable to the increase of two orders of magnitude in the specificity constant observed for RANBP2 with SUMO1[7]. Overall, these results suggest that $ZNF451_{2–56}$ catalyzes SUMO E3 ligase activity with a distinct preference for SUMO2.

ZNF451 preferentially binds SUMO2^{D}~UBC9–SUMO2^{B}

To better understand determinants for ZNF451 recognition of UBC9, SUMO2^{B} and SUMO2^{D}, fluorescence polarization experiments were conducted using Alexa488-modified ZNF451$_{2–56}$. UBC9 interacts with ZNF451 an apparent K_d of 10–16 μM while SUMO2 interacts with ZNF451 with a K_d of 120–150 μM (Fig. 2a,b). The latter values for interaction with SUMO2 are modestly higher than those reported for other SUMO–SIM interactions that are in the 1–100 μM range[22,42,43].

To determine how well ZNF451 interacts with thioester charged SUMO2^{D}~UBC9 we used two strategies, one employed SUMO2^{D}~RANGAP1–UBC9 as a mimic of charged E2 while the other employed a similar strategy as Plechanovová *et al.* through use of a C93K mutation in UBC9 to replace the thioester bond with slightly longer but stable SUMO2^{D}~UBC9$_{C93K}$ isopeptide bond[14]. ZNF451 interacts with SUMO2^{D}~UBC9$_{C93K}$ with a K_d of 3 μM. Perhaps consistent with RANGAP1 restricting the motion of SUMO2^{D} within the context of SUMO2^{D}~RANGAP1–UBC9 or with the longer isopeptide in SUMO2^{D}~UBC9$_{C93K}$ interfering with binding, ZNF451 binds the SUMO2^{D}~RANGAP1–UBC9 complex with a K_d of 0.2 μM. To diminish interactions between SUMO2 and the UBC9 backside surface that might occur in these mixtures, SUMO2^{D}~UBC9$_{C93K}$ and SUMO2^{D}~RANGAP1–UBC9 were generated using a SUMO2 D63R substitution that disrupts this interface[32]. SUMO2$^{D}{}_{D63R}$~UBC9$_{C93K}$ and SUMO2$^{D}{}_{D63R}$~RANGAP1–UBC9 interacts with ZNF451 with apparent K_d values of 1.3 μM and 0.4 μM, respectively.

Consistent with the K_d of 0.08–0.25 μM observed for the UBC9–SUMO1^{B} interaction[29,32], we measured an apparent K_d of 0.14 μM for the UBC9–SUMO2^{B} interaction (Supplementary Figure 1). We next sought to determine how well ZNF451 binds to UBC9–SUMO2^{B}. In this case, ZNF451 binds UBC9–SUMO2^{B} with an apparent K_d value of 2 μM, a value similar to that observed for SUMO2^{D}~UBC9$_{C93K}$ (Fig. 2a, b). In a final test, we added exogenous SUMO2 to preparations of SUMO2$^{D}{}_{D63R}$~UBC9$_{C93K}$ and SUMO2$^{D}{}_{D63R}$~RANGAP1–UBC9 to generate complexes containing SUMO^{B}. In these cases, ZNF451 interacts with SUMO2$^{D}{}_{D63R}$~UBC9$_{C93K}$–SUMO2^{B} and SUMO2$^{D}{}_{D63R}$~RANGAP1–UBC9–SUMO2^{B} with apparent K_d values of 0.4 μM and 0.05 μM, respectively, interactions that appear tighter when compared to those obtained in the absence of SUMO2^{B} (Fig. 2a, b). These interactions are specific as assessed by displacement of the Alexa488-labeled ZNF451-bound complex by unlabeled ZNF451$_{2–56}$ for both SUMO2$^{D}{}_{D63R}$~UBC9$_{C93K}$–SUMO2^{B} and SUMO2$^{D}{}_{D63R}$~RANGAP1–UBC9–SUMO2^{B} (Fig. 2c, d). Taken together, these experiments are fully consistent with a model in which ZNF451 interacts with a thioester-charged SUMO2^{D}~UBC9–SUMO2^{B} in E3 ligase catalysis.

Structure of a ZNF451–RANGAP1~SUMO2^{D}–E2–SUMO2^{B} complex

We proposed previously that a SUMO~RANGAP1–E2 complex mimics the active thioester charged E2~SUMO^{D} conformation in the presence of the E3 ligase RANBP2[7]. Subsequent structures in ubiquitin and NEDD8 pathways with Ub or NEDD8 attached to the E2 via isopeptide or ester adducts validated this hypothesis[10–15,44]. As such, we used RANGAP1~SUMO2^{D}–UBC9 as a surrogate for SUMO^{D}~UBC9 and obtained crystals of

ZNF451–SUMO2~RANGAP1–UBC9 that diffracted to 2.4 Å (Table 1 and Supplementary Fig. 2a). The complex contains one ZNF451 molecule and two SUMO2~RANGAP1–UBC9 complexes in the asymmetric unit (Supplementary Fig. 2b).

Visual inspection of the structure and analysis of protein contacts in the crystal using PISA[45] (Supplementary Fig. 2c) revealed that ZNF451 interacts with two molecules of SUMO2, $SUMO2^{D}$ and $SUMO2^{B}$, and one molecule of UBC9. The UBC9 that contacts ZNF451 interacts with $SUMO2^{D}$ and $SUMO2^{B}$, and buries 570 $Å^2$ and 670 $Å^2$ of accessible surface, respectively. The other molecule of UBC9 does not interact with ZNF451 and the interaction with $SUMO2^{B}$ is limited to a region around its active site as it is linked to the second $SUMO2^{B}$~RANGAP1–UBC9 complex. The SUMO2 molecule in second complex is thus donated to the other $SUMO2^{D}$~RANGAP1–UBC9 complex to form $SUMO2^{D}$~RANGAP1–UBC9–$SUMO^{B}$. The two UBC9 molecules make minor contacts to each other burying 238 $Å^2$ of accessible surface in an apparent lattice contact. The two RANGAP1–UBC9 interfaces are similar to each other and to that previously described[7,13,46]. On the basis of interactions observed in the structure and the biochemical studies described earlier, we propose that a biologically relevant complex (Fig. 3a) is composed of one ZNF451, one UBC9, and two molecules of SUMO2 with $SUMO2^{D}$ linked to the substrate RANGAP1 and $SUMO2^{B}$ coming from the second complex in the asymmetric unit.

As noted above, one molecule of SUMO2 interacts with ZNF451 and adopts a donor ($SUMO2^{D}$) conformation similar to that observed with RANBP2[7] (Fig. 3b) while the other SUMO2 molecule interacts with the backside of UBC9 ($SUMO2^{B}$) in a conformation similar to that observed in the UBC9–$SUMO1^{B}$ non-covalent complex[30] (Fig. 3c) and other UBC9–SUMO complexes[31,32]. Indeed, alignment of $SUMO2^{D}$ from ZNF451–$SUMO2^{D}$~RANGAP1–UBC9–$SUMO2^{B}$ to $SUMO2^{D}$ of the RANBP2–$SUMO2^{D}$~RANGAP1–UBC9 complex (pdb 3UIN[13]) results in a root mean square deviation (rmsd) of 1.3 Å for 76 matched Cα. The largest difference between $SUMO2^{D}$ moieties is within the C-terminus and omission of the five last residues of SUMO2 from the alignment decreases the rmsd from 1.3 to 0.6 Å. When UBC9 is used to align the complexes (Fig. 3b), the two $SUMO2^{D}$ molecules aligned with a rmsd of 3.7 Å for the same 71 matched Cα positions thus suggesting that $SUMO2^{D}$ adopts a similar fold and a comparable orientation in both E3 ligase complexes. Alignment of $SUMO2^{B}$ of the ZNF451–$SUMO2^{D}$~RANGAP1–UBC9–$SUMO2^{B}$ complex to the $SUMO1^{B}$ of the $SUMO1^{B}$–UBC9 non-covalent complex (pdb 2PE6[30]) results in a rmsd of 0.9 Å for 74 aligned Cα positions. If E2s are aligned, SUMO2 and SUMO1 align with a rmsd of 1.8 Å for the same 74 aligned Cα positions suggesting that these $SUMO^{B}$ molecules adopt similar folds and orientations in context of their interaction with UBC9.

SUMO–SIM interactions

The two ZNF451 SIMs interact with $SUMO2^{D}$ and $SUMO2^{B}$ through classical SUMO–SIM interactions and PISA analysis suggests that both SIM–SUMO2 interfaces are highly similar to each other in terms of interface area, $\Delta^{i}G$, and number of hydrogen bonds (Supplementary Fig. 2c). Despite these similarities, the N-terminal SIM of ZNF451 interacts with $SUMO2^{D}$ by forming a β-strand that runs antiparallel to the β-sheet of $SUMO2^{D}$ (Supplementary Fig.

3a) similar to RANBP2–SUMO2^{D} (ref. [13]; Supplementary Fig. 3b), while the C-terminal SIM of ZNF451 interacts with SUMO2^{B} by forming a β-strand that runs parallel to the β-sheet of SUMO2^{B} (Supplementary Fig. 3c). In addition to interactions involving main chain hydrogen bonds, several side chain contacts are observed between ZNF451 and SUMO2. Notably, ZNF451 SIM1 Glu36 and SIM2 Glu44 appear to form salt bridges with Arg50 of SUMO2^{D} and SUMO2^{B}, respectively. Furthermore, ZNF451 Gln32 is proximal to Lys33 of SUMO2^{D} and ZNF451 Ser35 is proximal to SUMO2^{D} Gln31. A comparison with RANBP2 reveals overall similarities between SUMO–SIM interactions (Supplementary Fig. 3b).

The PLRP motif in ZNF451 directly contacts the E2

The two SIMs of ZNF451 are separated by an intervening PLRP motif that is situated in a composite interface composed of SUMO2^{D}, UBC9 and SUMO2^{B} (Fig. 4a). The interaction between ZNF451 and E2 appears centered on an arginine residue that takes part in an intricate network of hydrogen bonds. Indeed, the ZNF451 Arg40 guanidinium is within direct hydrogen bonding distance of the side chain carboxylate of UBC9 Asp19 and backbone carbonyl oxygen of UBC9 His20. The guanidinium group of Arg40 is also within hydrogen bonding distance of four water molecules that, in turn, interact with the side chain carboxylate of UBC9 Asp19, the backbone carbonyl and amide groups of UBC9 His20, the side chain carboxylate of SUMO2^{B} Asp85 and the backbone carbonyl atom of SUMO2^{B} Gly24.

The two proline residues, Pro38 and Pro41 stack on each other thereby conferring the PLRP loop with its compact conformation. This loop conformation is not uncommon as some PLRP sequences adopt similar structures to that observed in ZNF451 despite being present in different chemical environments (Supplementary Fig. 3d). In the case of ZNF451, the PLRP motif appears to confer directionality to binding. Consistent with this hypothesis, the SUMO2^{B} and SUMO2^{D} are related by pseudo two-fold symmetry suggesting that SIM interactions could flip to allow N-terminal SIM interactions with SUMO2^{B} and C-terminal SIM interactions with SUMO2^{D}. Although a flip in orientation is sterically possible, it would presumably disrupt the intricate network of interactions between ZNF451 Arg40 and UBC9.

To determine if the PLRP motif is important for SUMO E3 ligase activity, alanine substitutions were introduced in this motif and the resulting proteins were assayed for SUMO2 conjugation to p53 in an end-point assay in single-turnover conditions. Alanine substitution mutants of ZNF451 Pro38 and Pro41 or Arg40 displayed reduced activity (Fig. 4b). In contrast, L39A substitution yielded activity similar to wild-type. Swapping L39 and R40 (LR to RL) resulted in diminished conjugation activity. To quantify the contribution of Pro38, Pro41 and Arg40 to ligase activity, two mutants were selected for further analysis, ZNF451$_{ALRA}$ and ZNF451$_{PLAP}$ (Fig. 4c and Supplementary Table 1). Alanine substitution of Pro38 and Pro41 disrupted the proline stack and displayed only 2.7% of the wild type ZNF451$_{2–56}$ activity while a mutant harboring a R40A substitution displayed 3.9% of the wild type ZNF451$_{2–56}$ activity. Although these substitutions did not diminish activity to levels observed in the absence of E3 (although the activity was still higher than in the absence of E3, by a factor of 3–4), these results highlight the importance of the PLRP motif

to ZNF451 ligase activity suggesting that Pro38 and Pro41 residues of the PLRP motif are important to maintain a loop conformation that allows Arg40 to interact with residues of UBC9 and $SUMO2^B$.

SUMO modification of ZNF451 increases activity

In our structure, the C-terminus of ZNF451 is located 8 Å (Cα-Cα distance) from the N-terminus of $SUMO2^B$ suggesting that we might be able to provide $SUMO2^B$ as a fusion to ZNF451 to bypass the need for exogenous SUMO2. We generated a chimeric $ZNF451_{2–55}SUMO2_{15–89}$ and tested it for activity. Consistent with our structure and prediction, the rate of SUMO2 conjugation in single-turnover conditions was faster in the absence of exogenous $SUMO2^B$ at every time-point for $ZNF451_{2–55}SUMO2_{15–89}$ as compared to $ZNF451_{2–56}$ alone (Supplementary Fig. 4). Notably, at 6.25 μM substrate, the measured rate of 0.065 s^{-1} using $ZNF451_{2–55}SUMO2_{15–89}$ was ~25 times faster than that of $ZNF451_{2–56}$.

Single-turnover assays using the $ZNF451_{2–55}$-$SUMO2_{15–89}$ chimeric protein differed from those of $ZNF451_{2–56}$ and resulted in more complex kinetics reminiscent of substrate inhibition (Supplementary Fig. 4). To achieve a better comparison between E3s, we utilized a lysine discharge assay similar to those used for thioester charged E2~Ub[10,11,47]. $ZNF451_{2–55}$-$SUMO2_{15–89}$ was three orders of magnitude more active than $ZNF451_{2–56}$ in lysine discharge assays in the absence of exogenous SUMO2 (Fig. 5a,c and Supplementary Table 2). Whereas addition of exogenous SUMO2 to $ZNF451_{2–56}$ increased the apparent rate by a factor of 50, addition of SUMO2 to $ZNF451_{2–55}$-$SUMO2_{15–89}$ had little effect (Fig. 5b,c and Supplementary Table 2). Interestingly, fusing ZNF451 to $SUMO2_{D63R}$ rendered it less active, both in the presence or absence of exogenous SUMO2. These results suggest that $SUMO2_{D63R}$, while impaired for E2 binding, may still bind and occlude the second ZNF451 SIM in the context of the $ZNF451_{2–55}$-$SUMO2_{15–89\ D63R}$ fusion to render it insensitive to addition of exogenous SUMO2.

Several studies identified ZNF451 as a substrate for SUMO2 conjugation[3,37–40]. As $ZNF451_{2–56}$ does not contain any lysine residues, this construct is not a target for SUMO2 conjugation. We therefore generated a longer $ZNF451_{2–110}$ construct that contains eight lysine residues, four of which act as SUMO acceptors *in vivo*[37]. $ZNF451_{2–110}$ is efficiently SUMO2-modified *in vitro* leading to the formation of mono- and poly-SUMO2 modified species that could be separated (Supplementary Fig. 5). Unmodified $ZNF451_{2–110}$ displays activities comparable to $ZNF451_{2–56}$ in presence or absence of exogenous $SUMO2_{15–89}$. Similar to the $ZNF451_{2–55}$-$SUMO2_{15–89}$ fusion, mono-modified $SUMO2_{15–89}$~$ZNF451_{2–110}$ was more than two order of magnitude more active than $ZNF451_{2–56}$ for SUMO2-conjugation in absence of exogenous SUMO2. Also analogous to the $ZNF451_{2–55}$-$SUMO2_{15–89}$ fusion, the SUMO2 D63R mutation strongly reduced the activity of conjugated $SUMO2_{15–89\ D63R}$~$ZNF451_{2–110}$. These results are consistent with the idea that SUMO2 modification of ZNF451 might increase its apparent activity by providing $SUMO^B$ in *cis* rather than relying on free SUMO for interaction with UBC9.

Discussion

There has been some debate as to whether certain SIM-containing proteins that increase SUMO conjugation are genuine E3 ligases[48]. Similarly to RING-based SUMO E3 ligases and RANBP2, ZNF451 contacts a charged E2 to maintain the donor SUMO in a closed conformation ready for discharge. Furthermore, mutations in the PLRP motif strongly decrease the catalytic efficiency of ZNF451. In other words, two SIMs are not sufficient to convert ZNF451 into a catalyst and it requires contacts with the E2 for activity. This result is in line with our structural data and it highlights the importance of the PLRP motif in establishing a network of direct and water-mediated interactions with a composite E2–SUMO interface. Taken together, these results suggest that the catalytic module within ZNF451 constitutes a *bona fide* member and new class of SUMO E3 ligase.

Buetow et al. proposed that Ub binding on the backside of thioester charged UBCH5~Ub increases the catalytic activity of the complex by restricting certain residues in helix α1 and in the α1β1 loop in a position more favorable for catalysis[10]. Analysis of equivalent positions in our structure did not reveal noticeable conformational changes when compared to the eighteen human structures of UBC9 that are devoid of $SUMO^B$ backside binding, in agreement with our observation that $SUMO2^B$ binding to thioester charged $SUMO2^D$~UBC9 does not increase the activity of the complex. Rather, ZNF451 appears to exploit the high affinity UBC9–$SUMO2^B$ non-covalent interaction by using its C-terminal SIM as an anchor to interact with $SUMO^B$ within $SUMO^D$~E2–$SUMO^B$ while its N-terminal SIM positions $SUMO^D$ in conjunction with the PLRP loop that contacts the E2. This mode of E2 interaction contrasts with PIAS proteins that use an SP-RING domain to physically associate to the E2 although studies suggest that interaction with E2–$SUMO^B$ may also contribute to the E3 ligase activities of PIAS proteins[49]. Interestingly, ZNF451 utilizes $SUMO^B$ to indirectly interact with the backside of UBC9 in thioester charged $SUMO^D$~E2–$SUMO^B$ while RANBP2 utilizes other structural elements beyond its SIM to penetrate the $SUMO^D$~E2 interface before wrapping additional elements and α-helices around to the backside of the E2.

Our biochemical data suggest that ZNF451 has a preference for SUMO2 over SUMO1. As modeling SUMO1 in place of SUMO2 in our structure does not result in steric occlusion, specificity might result from preferential SUMO2–SIM interactions with $SUMO^D$ and/or $SUMO^B$. Alternatively, the ZNF451 SIM-mediated interaction with SUMO1 may result in suboptimal positioning of the PLRP motif, in turn resulting in formation of less-productive complexes.

A recent comparative analysis of mass spectrometry data identified more than half of the lysine residues of ZNF451 as SUMO acceptor sites (43 identified sites out of 84 total lysine residues[37]). As we have shown that the N-terminal domain of ZNF451 has SUMO E3-ligase activity, it is possible that this domain facilitates SUMO-modification of these residues. The previous finding that the N-terminal domain of ZNF451 is SUMO-modified *in vitro* in a SIM-dependent manner is consistent with this idea[36]. Also in line with this idea is the existence of different ZNF451 isoforms that result from alternative splicing. These isoforms only share the first 62 residues of ZNF451 and one of them is followed by a domain that

shares sequence similarity with LAP2α domain[50]. The protein generated by this splicing isoform is also heavily SUMO-modified at 17 identified sites out of 32 available lysine residues[37].

As the catalytic module of ZNF451 is too small to engage substrates directly, it is likely that other regions of ZNF451 may be responsible for contacting exogenous substrates. The observation that three proteins possess the E3 ligase catalytic module of ZNF451 yet differ in their C-terminal domains raises the possibility that these proteins may have different substrate specificities. Furthermore, the N-terminal domain of KIAA1586 shows high sequence identity with the ZNF451 catalytic domain with one notable exception, the leucine residue in the PLRP motif is substituted by serine in KIAA1586. Our mutational data suggests that this position is not important for activity, so it is possible that KIAA1586 may also possess SUMO E3 ligase activity.

Finally, our biochemical data suggest that SUMO modification of $ZNF451_{2–110}$ increases its catalytic efficiency, although SUMO-modification of other sites or SUMO-modification of the same site in the context of full-length ZNF451 may result in different effects. SUMO-modification of multiple sites may however eventually decrease ZNF451 ligase activity by masking both SIMs thus precluding interaction with activated SUMO~E2. Regulation of ZNF451 may be even more complex as 29 of its 43 available SUMO-acceptor lysine residues can also act as Ub acceptor sites[51]. Finally, two serine residues at the C-terminal of the second SIM belong to CK2 consensus sites and phosphorylation of those sites could generate a phosphoSIM and potentiate SUMO–SIM interactions as observed in other systems[42,43,52].

Online Methods

Cloning, protein expression and purification

Expression and purification of human E1ΔCT ($SAE1_{1–349}$–$UBA2_{1–550}$), $SUMO1_{1–97}$, $SUMO1_{1–97\ S9C\ C52A}$, $SUMO2_{1–93}$, $p53_{320–393}$ (tetramerization domain) and $RANGAP1_{419–587}$ were performed as described previously[7,46,53]. Untagged human E2 (UBC9) was cloned in pET-11c, expressed in BL21 DE3 Codon Plus RIL (Stratagene) cells and purified by cation exchange chromatography on SP Sepharose resin (GE Healthcare) and size exclusion chromatography on a Superdex 75 column (GE Healthcare) equilibrated with 20 mM Tris-HCl pH 8, 350 mM NaCl and 1 mM 2-mercaptoethanol. $ZNF451_{2–56}$ was expressed in BL21 DE3 Codon Plus RIL cells as an MBP fusion protein using the pLou3-$ZNF451_{2–56}$ plasmid kindly provided by Dr. A. Pichler. Cells were grown in baffled flasks using Super broth media (Teknova) and induced by addition of isopropyl-β-D-thiogalactopyranoside (IPTG) to a final concentration of 0.3 mM followed by incubation of the cultures at 18°C for 15 h. The MBP–$ZNF451_{2–56}$ protein was purified by affinity chromatography using Ni-NTA resin (QIAGEN) and by size exclusion chromatography using a Superdex 200 column (GE Healthcare) equilibrated with 20 mM Tris-HCl pH 8, 350 mM NaCl and 1 mM 2-mercaptoethanol. MBP was cleaved using a TEV protease and removed by rebinding to Ni-NTA resin. $ZNF451_{2–56}$ was further purified by anion exchange chromatography using a MonoQ column (GE Healthcare).

$SUMO2_{1–93\ A2C\ C48A}$, $SUMO2_{1–93\ D63R}$, $UBC9_{K14R}$, $UBC9_{C93K}$ and $ZNF451_{2–56}$ PLRP mutants were obtained by PCR mutagenesis and were expressed and purified as their non-mutated counterparts. The $ZNF451_{2–55}SUMO2_{15–89}$ fusion was obtained using plasmids coding for $ZNF451_{2–56}$ and SUMO2 as PCR templates. The chimeric DNA was inserted after the TEV site of a pTrx28 plasmid. pTrx28 is a modified pET-28b-based plasmid that allows the production of proteins as His_6-thioredoxin fusions with a TEV cleavage site immediately following the thioredoxin sequence. $ZNF451_{2–110}$ was obtained by PCR using a pLou3-$ZNF451_{2–247}$ plasmid as a template and inserted in pTrx28. A $CysZNF451_{2–56}$ construct was obtained by inserting a $ZNF451_{2–56}$ construct with an engineered cysteine at its N-terminus after the TEV cleavage site of a pTrx28 vector. These three proteins were expressed in BL21 DE3 Codon Plus RIL cells as for $ZNF451_{2–56}$ and were purified by affinity chromatography using Ni-NTA resin and by size exclusion using Superdex 75 equilibrated with 20 mM Tris-HCl pH 8, 350 mM NaCl and 1 mM 2-mercaptoethanol. Thioredoxin was cleaved using a TEV protease and removed by rebinding to Ni-NTA resin.

$SUMO2_{15–93}$~RANGAP1 and $SUMO2_{15–93\ D63R}$~RANGAP1 conjugation reactions were performed as described[13]. ATP and magnesium were removed by applying the conjugation reaction on a HiPrep Desalting column (GE Healthcare) equilibrated with 20 mM Tris pH 8, 50 mM NaCl and 1 mM 2-mercaptoethanol. $SUMO2_{15–93}$~RANGAP1 and $SUMO2_{15–93\ D63R}$~RANGAP1 were subsequently purified on a MonoQ column. $UBC9_{C93K}$ conjugation reaction was performed for 15 h at 37°C using 20 mM Bis-Tris Propane pH 9.5, 50 mM NaCl, 5 mM $MgCl_2$, 3 mM DTT, 2 mM ATP, 400 nM E1ΔCT, 90 μM $SUMO2_{15–93}$ or $SUMO2_{15–93\ D63R}$ and 90 μM $UBC9_{C93K}$. $SUMO2_{15–93}$~$UBC9_{C93K}$ was applied on a HiPrep Desalting column equilibrated with 20 mM Tris pH 8, 50 mM NaCl and 1 mM 2-mercaptoethanol and purified on a MonoQ column. $SUMO2_{15–93\ D63R}$~$UBC9_{C93K}$ was purified on a Superose 12 column (GE Healthcare). $SUMO2_{15–93}$~$ZNF451_{2–110}$ and $SUMO2_{15–93\ D63R}$~$ZNF451_{2–110}$ conjugation reactions were performed for 1 h at 37°C using 20 mM HEPES pH 7.5, 50 mM NaCl, 5 mM $MgCl_2$, 0.1% Tween-20, 3 mM DTT, 5 mM ATP, 200 nM E1ΔCT, 500 nM $UBC9_{K14R}$, 34 μM $SUMO2_{15–93}$ and 28 μM $ZNF451_{2–110}$. $SUMO2_{15–93}$~$ZNF451_{2–110}$ and $SUMO2_{15–93\ D63R}$~$ZNF451_{2–110}$ were then passed on a HiPrep Desalting column equilibrated with 20 mM Tris pH 8, 50 mM NaCl and 1 mM 2-mercaptoethanol and subsequently purified on a MonoQ column.

Single-turnover assay

$SUMO1_{1–97\ S9C\ C52A}$ and $SUMO2_{1–93\ A2C\ C48A}$ were labeled with Alexa488-maleimide (Life Technologies) according to the manufacturer instructions. SUMO~UBC9 thioester adducts were prepared at 37°C in 20 mM Tris pH 8.5, 250 mM NaCl, 0.1% Tween 20, 5 mM $MgCl_2$, 0.4 mM DTT and 1 mM ATP using 1 μM E1ΔCT, 10 μM untagged UBC9 and 10 μM Alexa488-labeled $SUMO1_{1–97\ S9C\ C52A}$ or 10 μM Alexa 488-labeled $SUMO2_{1–93\ A2C\ C48A}$. After 7 minutes, the reactions were passed on Bio-Spin P-6 columns (Bio-Rad) equilibrated with 50 mM sodium citrate pH 5.5 and 50 mM NaCl. Glycerol was added to a final concentration of 10% and aliquots of this solution were flash-cooled in liquid nitrogen and kept at –80°C until needed.

Single-turnover assays were conducted at 0°C in 20 mM HEPES pH 7.5, 50 mM NaCl, 0.1% Tween-20 and 5 mM EDTA and were initiated by adding thioester charged SUMO1~UBC9 or SUMO2~UBC9 to serially-diluted $p53_{320–393}$ (tetramerization domain) in the absence or presence of 100 nM $ZNF451_{2–56}$ and/or $SUMO2_{15–89}$ or $SUMO1_{19–94}$. At indicated time points, aliquots were removed and rapidly quenched in a buffer containing 50 mM HEPES pH 7.5, 2 % SDS, 4M urea, 10 % glycerol and 0.25 % bromophenol blue. Samples were migrated at 180 V on a 12 % SDS-PAGE gel with MES running buffer (Life Technologies). Gels were imaged on a Typhoon 9500 (GE Healthcare) with a 473 nm laser and a LPB filter and bands were quantified using ImageJ (NIH). Eight different p53 concentrations were used with three time points per concentration. Experiments were performed in triplicate. Time points where more than 80% of thioester charged SUMO~UBC9 was consumed were excluded from the analysis. Data was fitted to the equation $v = V_{max}[S]/(K_d + [S])$ in Prism 6 (GraphPad), where $V_{max} = k_2[E]_t$, k_2 is the rate constant, $[E]_t$ is the SUMO~E2 thioester concentration, K_d is the apparent dissociation constant, and [S] is the substrate concentration.

Fluorescence polarization

A Cys-$ZNF451_{2–56}$ protein containing only one cysteine residue at its N-terminus was labeled with Alexa488-maleimide according to the manufacturer instructions. All proteins used in fluorescence polarization experiments were passed on a Bio-Spin P-6 columns equilibrated with 20 mM HEPES pH 7.5, 50 mM NaCl and 0.1% Tween-20. Fluorescence polarization experiments were performed at 23°C using a SpectraMax M5 (Molecular Devices) microplate reader with excitation, emission, and cutoff wavelengths of 485, 525 and 515 nm, respectively. Measurements were performed in 384-well microplates using 20 µl reactions containing 100 nM Alexa488 labeled Cys–$ZNF451_{2–56}$ and serially diluted target proteins. Experiments were performed in technical triplicates and analyzed in Prism 6 using a single site binding model accounting for ligand depletion as described[54]. Displacement experiments were performed by incubating 1 µM $SUMO2_{15–93\ D63R}$~$RANGAP1–UBC9–SUMO2_{15–89}$ or 3 µM $SUMO2_{15–93\ D63R}$~$UBC9_{C93K}–SUMO2_{15–89}$ with 200 nM Alexa488 labeled Cys-$ZNF45_{12–56}$ and adding an equal volume of serially diluted unlabeled $ZNF451_{2–56}$ before measurement.

Crystallization and X-ray data collection

$SUMO2_{15–93}$~$RANGAP1_{419–587}$ was mixed with $UBC9_{K14R}$ and $ZNF451_{2–56}$ in a 1:1:1 molar ratio and purified by size-exclusion chromatography using a Superose 6 (GE Healthcare) column in a buffer consisting of 20 mM Tris pH 8, 50 mM NaCl and 1 mM 2-mercaptoethanol. The complex was concentrated to 20 mg/ml and crystallized at 291 K by the hanging-drop vapour-diffusion method by mixing 2 µl of the complex with 2 µl of a reservoir solution consisting of 6% (w/v) PEG 8,000, 0.2 M ammonium citrate and 0.1 M HEPES pH 7.5. Crystals were cryoprotected by soaking into a solution containing 14% (w/v) PEG 8,000, 16% (v/v) ethylene glycol, 0.2 M ammonium citrate and 0.1 M HEPES pH 7.5 and snap-cooled in liquid nitrogen. Data collection was performed at 100 K at the X29 beamline of the NSLS using a ADSC Q315 detector and a wavelength of 1.075 Å. Indexing and integration of the diffraction data were performed using XDS[55]. Due to

diffraction anisotropy, the scaling was performed using XSCALE and the Diffraction Anisotropy Server[56] (UCLA). The resolution was cut to 2.4 Å to maintain a high completeness in the high resolution bins. Molecular replacement was performed using PHENIX[57] and the crystal structure of RANGAP1~SUMO2 with UBC9 (pdb 3UIO[13]) as a search model. Refinement and model building were performed using PHENIX[57] and COOT[58], respectively. Residues 30–50 of ZNF451 are visible in the electron density maps. The geometry of the structure was analyzed using MolProbity[59]. 97.4% of the residues are in favored configuration with no Ramachandran outlier. The structure has a clash score is 1.62 (100th percentile) and a Molprobity score of 1.20 (100th percentile). Figures were prepared with PyMOL (http://www.pymol.org/).

Lysine discharge assay

Lysine discharge assays were performed in triplicate at 0°C and initiated by mixing thioester charged UBC9~Alexa488-labeled $SUMO2_{1–93\ A2C\ C48A}$ and the E3 with or without 3 μM $SUMO2_{15–89}$ in presence or absence of 10 mM L-lysine. The final buffer contains 20 mM HEPES pH 7.5, 50 mM NaCl, 0.1% Tween-20, 5 mM EDTA, 0 or 10 mM L-Lysine, 0 or 100 nM E3 and 0 or 3 μM $SUMO2_{15–89}$. At indicated time-points, the reactions were rapidly quenched in a buffer containing 50 mM HEPES pH 7.5, 2 % SDS, 4 M urea, 10% glycerol and 0.25 % bromophenol blue and migrated at 180V on a 12 % SDS-PAGE gel with MES running buffer. The gels were imaged on a Typhoon 9500 with a 473 nM laser and LPB filter. Individual bands were then quantified using ImageJ and Alexa488-labeled SUMO2 standards. Rates were obtained by fitting the data using linear regression analysis in Prism 6. Accumulation of lysine-bound SUMO was measured rather than the depletion of thioester charged UBC9~SUMO2 as the former displayed less variability.

Supplementary Material

Refer to Web version on PubMed Central for supplementary material.

Acknowledgements

We would like to thank the A. Pichler lab for providing the pLou3-$ZNF451_{2–56}$ and pLou3-$ZNF451_{2–247}$ plasmids, and member of the A. Pichler and C.D. Lima labs for discussion. Data for this study were measured at beamline X29 of the National Synchrotron Light Source. Financial support comes principally from the Offices of Biological and Environmental Research and of Basic Energy Sciences of the US Department of Energy (DOE), and from the National Center for Research Resources (P41RR012408) and the National Institute of General Medical Sciences (NIGMS; P41GM103473) of the US National Institutes of Health (NIH). This work is also based upon research conducted at the Northeastern Collaborative Access Team beamlines, which are funded by the NIGMS from the NIH (P41 GM103403). The Pilatus 6M detector on 24-ID-C beam line is funded by a NIH-ORIP HEI grant (S10 RR029205). This research used resources of the Advanced Photon Source, a DOE Office of Science User Facility operated for the DOE Office of Science by Argonne National Laboratory under Contract No. DE-AC02-06CH11357. Research reported in this publication was supported in part by the NIGMS of the NIH under award number GM065872 (C.D.L.) and the NIH/NCI Cancer Center Support Grant P30 CA008748. The content is solely the responsibility of the authors and does not necessarily represent the official views of the NIH. A.P. is supported by the Max Planck Society and the Deutsche Forschungsgemeinschaft (DFG-SPP1365 PI 917/2-1). L.C. is supported in part by a fellowship from the Fonds de Recherche du Québec - Santé. C.D.L. is an Investigator of the Howard Hughes Medical Institute.

References

1. Kerscher O, Felberbaum R, Hochstrasser M. Modification of proteins by ubiquitin and ubiquitin-like proteins. Annu Rev Cell Dev Biol. 2006; 22:159–180. [PubMed: 16753028]
2. Streich FC Jr, Lima CD. Structural and functional insights to ubiquitin-like protein conjugation. Annu Rev Biophys. 2014; 43:357–379. [PubMed: 24773014]
3. Hendriks IA, et al. Uncovering global SUMOylation signaling networks in a site-specific manner. Nat Struct Mol Biol. 2014; 21:927–936. [PubMed: 25218447]
4. Sampson DA, Wang M, Matunis MJ. The small ubiquitin-like modifier-1 (SUMO-1) consensus sequence mediates Ubc9 binding and is essential for SUMO-1 modification. J Biol Chem. 2001; 276:21664–21669. [PubMed: 11259410]
5. Tatham MH, et al. Polymeric chains of SUMO-2 and SUMO-3 are conjugated to protein substrates by SAE1/SAE2 and Ubc9. J Biol Chem. 2001; 276:35368–35374. [PubMed: 11451954]
6. Saitoh H, Hinchey J. Functional heterogeneity of small ubiquitin-related protein modifiers SUMO-1 versus SUMO-2/3. J Biol Chem. 2000; 275:6252–6258. [PubMed: 10692421]
7. Reverter D, Lima CD. Insights into E3 ligase activity revealed by a SUMO-RanGAP1-Ubc9-Nup358 complex. Nature. 2005; 435:687–692. [PubMed: 15931224]
8. Pruneda JN, et al. Structure of an E3:E2~Ub complex reveals an allosteric mechanism shared among RING/U-box ligases. Mol Cell. 2012; 47:933–942. [PubMed: 22885007]
9. Branigan E, Plechanovova A, Jaffray EG, Naismith JH, Hay RT. Structural basis for the RING-catalyzed synthesis of K63-linked ubiquitin chains. Nat Struct Mol Biol. 2015
10. Buetow L, et al. Activation of a primed RING E3-E2-ubiquitin complex by non-covalent ubiquitin. Mol Cell. 2015; 58:297–310. [PubMed: 25801170]
11. Dou H, Buetow L, Sibbet GJ, Cameron K, Huang DT. BIRC7-E2 ubiquitin conjugate structure reveals the mechanism of ubiquitin transfer by a RING dimer. Nat Struct Mol Biol. 2012; 19:876–883. [PubMed: 22902369]
12. Dou H, Buetow L, Sibbet GJ, Cameron K, Huang DT. Essentiality of a non-RING element in priming donor ubiquitin for catalysis by a monomeric E3. Nat Struct Mol Biol. 2013; 20:982–986. [PubMed: 23851457]
13. Gareau JR, Reverter D, Lima CD. Determinants of small ubiquitin-like modifier 1 (SUMO1) protein specificity, E3 ligase, and SUMO-RanGAP1 binding activities of nucleoporin RanBP2. J Biol Chem. 2012; 287:4740–4751. [PubMed: 22194619]
14. Plechanovová A, Jaffray EG, Tatham MH, Naismith JH, Hay RT. Structure of a RING E3 ligase and ubiquitin-loaded E2 primed for catalysis. Nature. 2012; 489:115–120. [PubMed: 22842904]
15. Scott DC, et al. Structure of a RING E3 trapped in action reveals ligation mechanism for the ubiquitin-like protein NEDD8. Cell. 2014; 157:1671–1684. [PubMed: 24949976]
16. Klug H, et al. Ubc9 sumoylation controls SUMO chain formation and meiotic synapsis in Saccharomyces cerevisiae. Mol Cell. 2013; 50:625–636. [PubMed: 23644018]
17. Wickliffe KE, Lorenz S, Wemmer DE, Kuriyan J, Rape M. The mechanism of linkage-specific ubiquitin chain elongation by a single-subunit E2. Cell. 2011; 144:769–781. [PubMed: 21376237]
18. Hochstrasser M. SP-RING for SUMO: new functions bloom for a ubiquitin-like protein. Cell. 2001; 107:5–8. [PubMed: 11595179]
19. Reindle A, et al. Multiple domains in Siz SUMO ligases contribute to substrate selectivity. J Cell Sci. 2006; 119:4749–4757. [PubMed: 17077124]
20. Pichler A, Knipscheer P, Saitoh H, Sixma TK, Melchior F. The RanBP2 SUMO E3 ligase is neither HECT- nor RING-type. Nat Struct Mol Biol. 2004; 11:984–991. [PubMed: 15378033]
21. Hecker CM, Rabiller M, Haglund K, Bayer P, Dikic I. Specification of SUMO1- and SUMO2-interacting motifs. J Biol Chem. 2006; 281:16117–16127. [PubMed: 16524884]
22. Song J, Durrin LK, Wilkinson TA, Krontiris TG, Chen Y. Identification of a SUMO-binding motif that recognizes SUMO-modified proteins. Proc Natl Acad Sci U S A. 2004; 101:14373–14378. [PubMed: 15388847]

23. Song J, Zhang Z, Hu W, Chen Y. Small ubiquitin-like modifier (SUMO) recognition of a SUMO binding motif: a reversal of the bound orientation. J Biol Chem. 2005; 280:40122–40129. [PubMed: 16204249]
24. Guervilly JH, et al. The SLX4 complex is a SUMO E3 ligase that impacts on replication stress outcome and genome stability. Mol Cell. 2015; 57:123–137. [PubMed: 25533188]
25. Merrill JC, et al. A role for non-covalent SUMO interaction motifs in Pc2/CBX4 E3 activity. PLoS One. 2010; 5:e8794. [PubMed: 20098713]
26. Ouyang J, et al. Noncovalent interactions with SUMO and ubiquitin orchestrate distinct functions of the SLX4 complex in genome maintenance. Mol Cell. 2015; 57:108–122. [PubMed: 25533185]
27. Yang SH, Sharrocks AD. The SUMO E3 ligase activity of Pc2 is coordinated through a SUMO interaction motif. Mol Cell Biol. 2010; 30:2193–2205. [PubMed: 20176810]
28. Liu Q, et al. The binding interface between an E2 (UBC9) and a ubiquitin homologue (UBL1). J Biol Chem. 1999; 274:16979–16987. [PubMed: 10358047]
29. Tatham MH, et al. Role of an N-terminal site of Ubc9 in SUMO-1, −2, and −3 binding and conjugation. Biochemistry. 2003; 42:9959–9969. [PubMed: 12924945]
30. Capili AD, Lima CD. Structure and analysis of a complex between SUMO and Ubc9 illustrates features of a conserved E2-Ubl interaction. J Mol Biol. 2007; 369:608–618. [PubMed: 17466333]
31. Duda DM, et al. Structure of a SUMO-binding-motif mimic bound to Smt3p–Ubc9p: conservation of a non-covalent ubiquitin-like protein-E2 complex as a platform for selective interactions within a SUMO pathway. J Mol Biol. 2007; 369:619–630. [PubMed: 17475278]
32. Knipscheer P, van Dijk WJ, Olsen JV, Mann M, Sixma TK. Noncovalent interaction between Ubc9 and SUMO promotes SUMO chain formation. EMBO J. 2007; 26:2797–2807. [PubMed: 17491593]
33. Brzovic PS, Lissounov A, Christensen DE, Hoyt DW, Klevit RE. A UbcH5/ubiquitin noncovalent complex is required for processive BRCA1-directed ubiquitination. Mol Cell. 2006; 21:873–880. [PubMed: 16543155]
34. Eddins MJ, Carlile CM, Gomez KM, Pickart CM, Wolberger C. Mms2-Ubc13 covalently bound to ubiquitin reveals the structural basis of linkage-specific polyubiquitin chain formation. Nat Struct Mol Biol. 2006; 13:915–920. [PubMed: 16980971]
35. Hibbert RG, Huang A, Boelens R, Sixma TK. E3 ligase Rad18 promotes monoubiquitination rather than ubiquitin chain formation by E2 enzyme Rad6. Proc Natl Acad Sci U S A. 2011; 108:5590–5595. [PubMed: 21422291]
36. Karvonen U, Jaaskelainen T, Rytinki M, Kaikkonen S, Palvimo JJ. ZNF451 is a novel PML body- and SUMO-associated transcriptional coregulator. J Mol Biol. 2008; 382:585–600. [PubMed: 18656483]
37. Hendriks IA, D'Souza RC, Chang JG, Mann M, Vertegaal AC. System-wide identification of wild-type SUMO-2 conjugation sites. Nat Commun. 2015; 6:7289. [PubMed: 26073453]
38. Matic I, et al. Site-specific identification of SUMO-2 targets in cells reveals an inverted SUMOylation motif and a hydrophobic cluster SUMOylation motif. Mol Cell. 2010; 39:641–652. [PubMed: 20797634]
39. Schimmel J, et al. Uncovering SUMOylation dynamics during cell-cycle progression reveals FoxM1 as a key mitotic SUMO target protein. Mol Cell. 2014; 53:1053–1066. [PubMed: 24582501]
40. Tammsalu T, et al. Proteome-wide identification of SUMO2 modification sites. Sci Signal. 2014; 7:rs2. [PubMed: 24782567]
41. Eisenhardt N, et al. A novel vertebrate SUMO enzyme family reveals insights into SUMO-chain assembly. Nat. Struct. Mol. Biol. 2015 Nov 2.
42. Cappadocia L, et al. Structural and functional characterization of the phosphorylation-dependent interaction between PML and SUMO1. Structure. 2015; 23:126–138. [PubMed: 25497731]
43. Chang CC, et al. Structural and functional roles of Daxx SIM phosphorylation in SUMO paralog-selective binding and apoptosis modulation. Mol Cell. 2011; 42:62–74. [PubMed: 21474068]
44. Lima CD, Schulman BA. Structural biology: A protein engagement RING. Nature. 2012; 489:43–44. [PubMed: 22955611]

45. Krissinel E, Henrick K. Inference of macromolecular assemblies from crystalline state. J Mol Biol. 2007; 372:774–797. [PubMed: 17681537]
46. Bernier-Villamor V, Sampson DA, Matunis MJ, Lima CD. Structural basis for E2-mediated SUMO conjugation revealed by a complex between ubiquitin-conjugating enzyme Ubc9 and RanGAP1. Cell. 2002; 108:345–356. [PubMed: 11853669]
47. Pickart CM, Rose IA. Functional heterogeneity of ubiquitin carrier proteins. J Biol Chem. 1985; 260:1573–1581. [PubMed: 2981864]
48. Parker JL, Ulrich HD. SIM-dependent enhancement of substrate-specific SUMOylation by a ubiquitin ligase in vitro. Biochem J. 2014; 457:435–440. [PubMed: 24224485]
49. Mascle XH, et al. Identification of a non-covalent ternary complex formed by PIAS1, SUMO1, and UBC9 proteins involved in transcriptional regulation. J Biol Chem. 2013; 288:36312–36327. [PubMed: 24174529]
50. Abascal F, Tress ML, Valencia A. Alternative splicing and co-option of transposable elements: the case of TMPO/LAP2alpha and ZNF451 in mammals. Bioinformatics. 2015; 31:2257–2261. [PubMed: 25735770]
51. Udeshi ND, et al. Refined preparation and use of anti-diglycine remnant (K-epsilon-GG) antibody enables routine quantification of 10,000s of ubiquitination sites in single proteomics experiments. Mol Cell Proteomics. 2013; 12:825–831. [PubMed: 23266961]
52. Scaglioni PP, et al. A CK2-dependent mechanism for degradation of the PML tumor suppressor. Cell. 2006; 126:269–283. [PubMed: 16873060]
53. Yunus, AA.; Lima, CD. Purification of SUMO Conjugating Enzymes and Kinetic Analysis of Substrate Conjugation. In: Ulrich, HD., editor. Methods in Molecular Biology: SUMO Protocols. Vol. 497. 2009. p. 167-186.
54. Armstrong AA, Mohideen F, Lima CD. Recognition of SUMO-modified PCNA requires tandem receptor motifs in Srs2. Nature. 2012; 483:59–63. [PubMed: 22382979]
55. Kabsch W. Xds. Acta Crystallogr D Biol Crystallogr. 2010; 66:125–132. [PubMed: 20124692]
56. Strong M, et al. Toward the structural genomics of complexes: crystal structure of a PE/PPE protein complex from Mycobacterium tuberculosis. Proc Natl Acad Sci U S A. 2006; 103:8060–8065. [PubMed: 16690741]
57. Adams PD, et al. PHENIX: a comprehensive Python-based system for macromolecular structure solution. Acta Crystallogr D Biol Crystallogr. 2010; 66:213–221. [PubMed: 20124702]
58. Emsley P, Lohkamp B, Scott WG, Cowtan K. Features and development of Coot. Acta Crystallogr D Biol Crystallogr. 2010; 66:486–501. [PubMed: 20383002]
59. Chen VB, et al. MolProbity: all-atom structure validation for macromolecular crystallography. Acta Crystallogr D Biol Crystallogr. 2010; 66:12–21. [PubMed: 20057044]

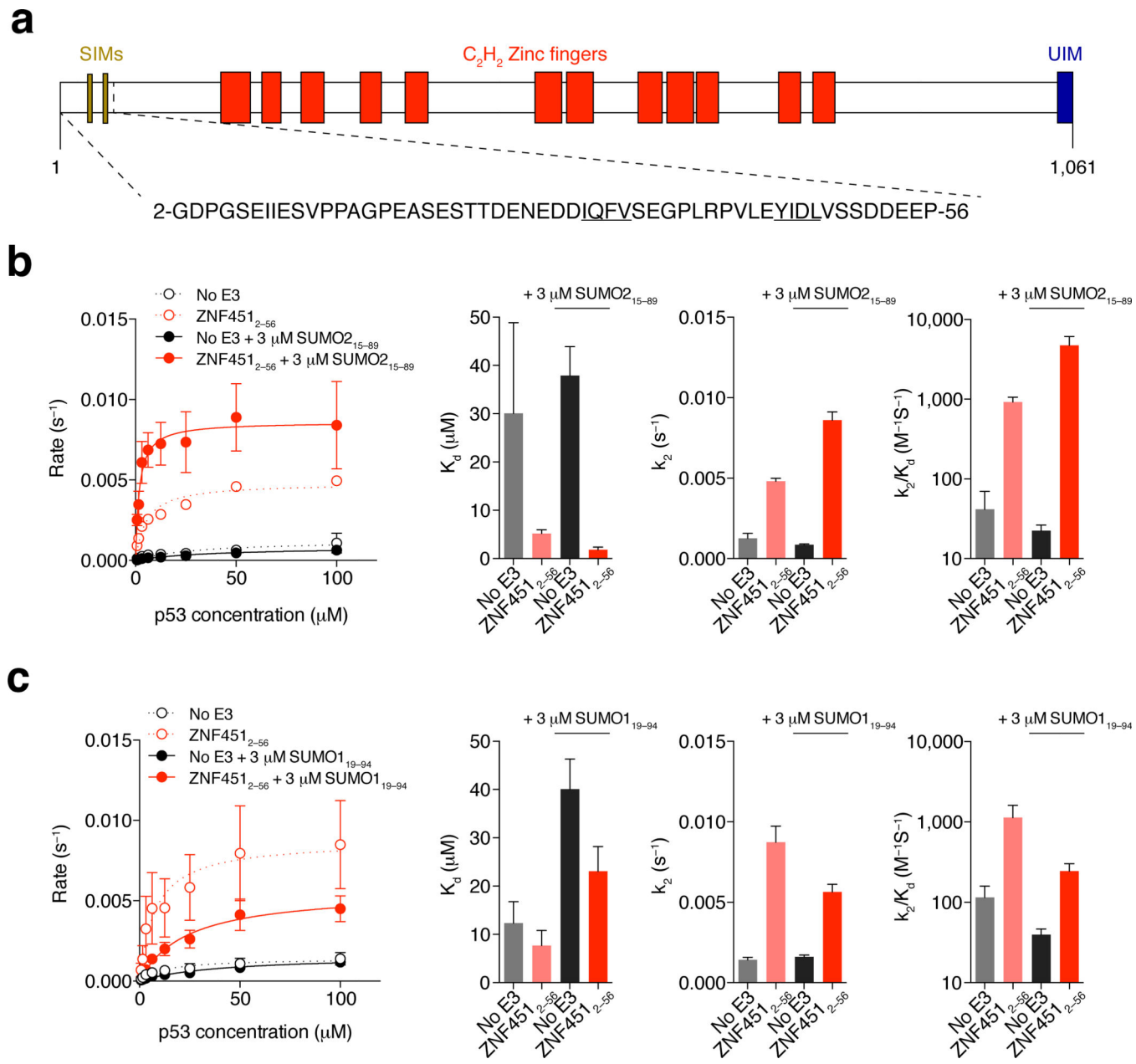

Figure 1.

The N-terminal domain of ZNF451 encompassing two SIMs displays SUMO2 conjugation activity. (**a**) Diagram showing the domain organization of ZNF451. Colored boxes represent predicted domains or motifs. ZNF451 contains two SUMO-Interacting Motifs (SIMs), twelve C_2H_2-type zinc fingers and one Ubiquitin interacting motif (UIM). The sequence of the fragment (residues 2–56) used in this study is displayed below the diagram. Residues belonging to the two SIMs are underlined. (**b**) Single-turnover conjugation rates of SUMO2 to p53 tetramerization domain (residues 320–393) in presence or absence of 100 nM $ZNF451_{2–56}$ and 3 μM $SUMO2_{15–89}$. Left, plot showing the initial rate of SUMO conjugation versus p53 concentration. Data show mean ± s.d. (n=3 technical replicates). Representative gels are shown in Supplementary Data Set 1. Right, histograms presenting

k_2, K_d and specificity (k_2/K_d) constant for SUMO2 conjugation to p53. Histograms show mean ± s.e.m. The histogram for the specificity constant is in logarithmic scale. (**c**) Single-turnover conjugation rates of SUMO1 to the p53 tetramerization domain in presence or in absence of 100 nM $ZNF451_{2–56}$ and 3 μM $SUMO1_{19–94}$ presented as in Figure 1b. Data show mean ± s.d. (n=3 technical replicates). Representative gels are shown in Supplementary Data Set 1.

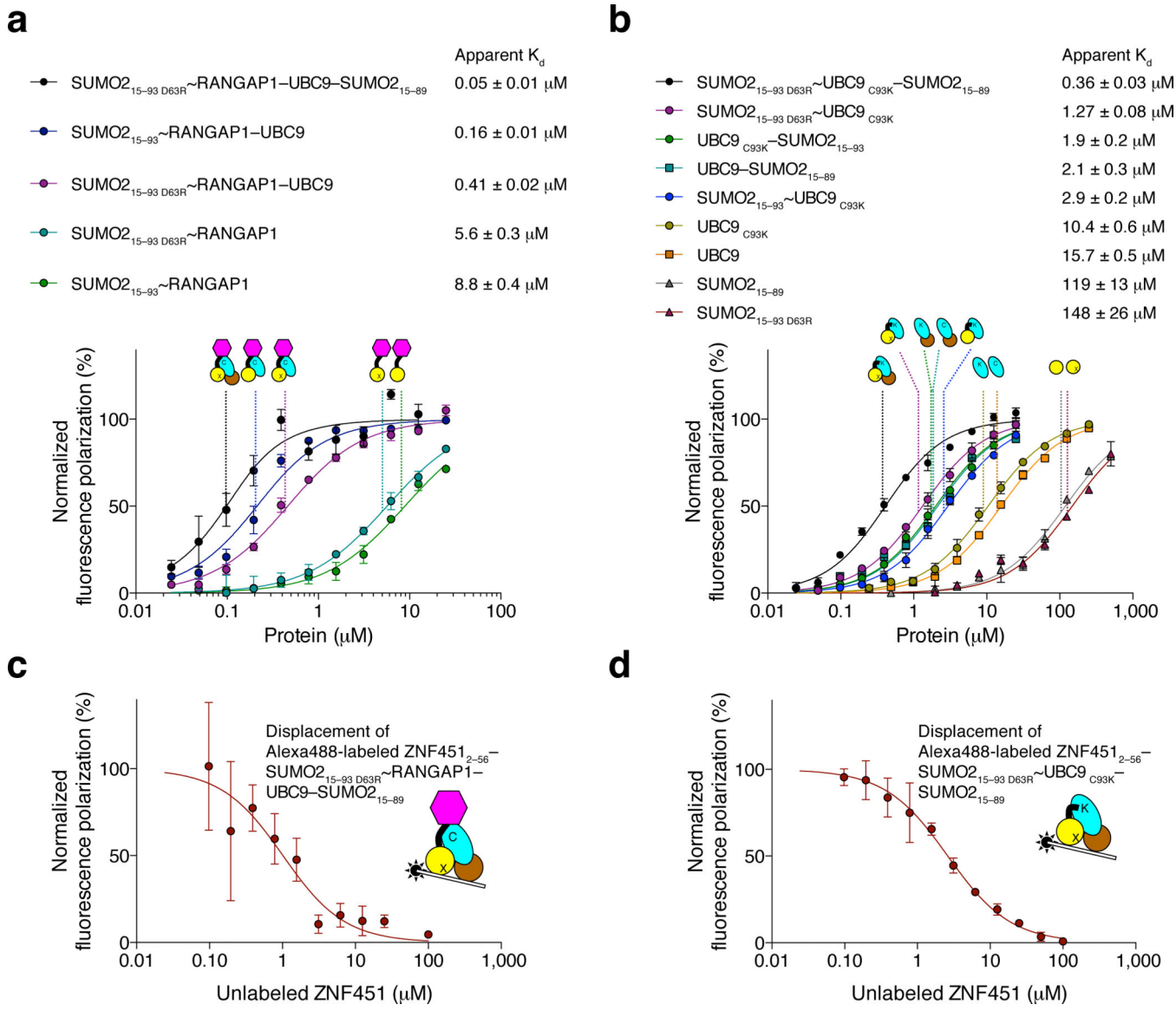

Figure 2.

ZNF451 preferentially binds a charged and backside-bound UBC9. (**a,b**) Fluorescence polarization assays performed using 100 nM Alexa488-labeled CysZNF451$_{2–56}$ and serially diluted RANGAP1-containing protein complexes (**a**) or the indicated protein complexes (**b**). Data is mean ± s.d. (n=3 technical replicates). Data was fitted to a single site binding model accounting for ligand depletion. No detectable binding was measured for RANGAP1 alone. (**c,d**) Displacement assay of the Alexa488-labeled CysZNF451$_{2–56}$–SUMO2$_{15–93\ D63R}$~RANGAP1–UBC9–SUMO2$_{15–89}$ complex (**c**) or the CysZNF451$_{2–56}$–SUMO2$_{15–93\ D63R}$~UBC9$_{C93K}$–SUMO2$_{15–89}$ complex (**d**) using serially diluted unlabeled ZNF451$_{2–56}$. Data is mean ± s.d. (n=3 technical replicates).

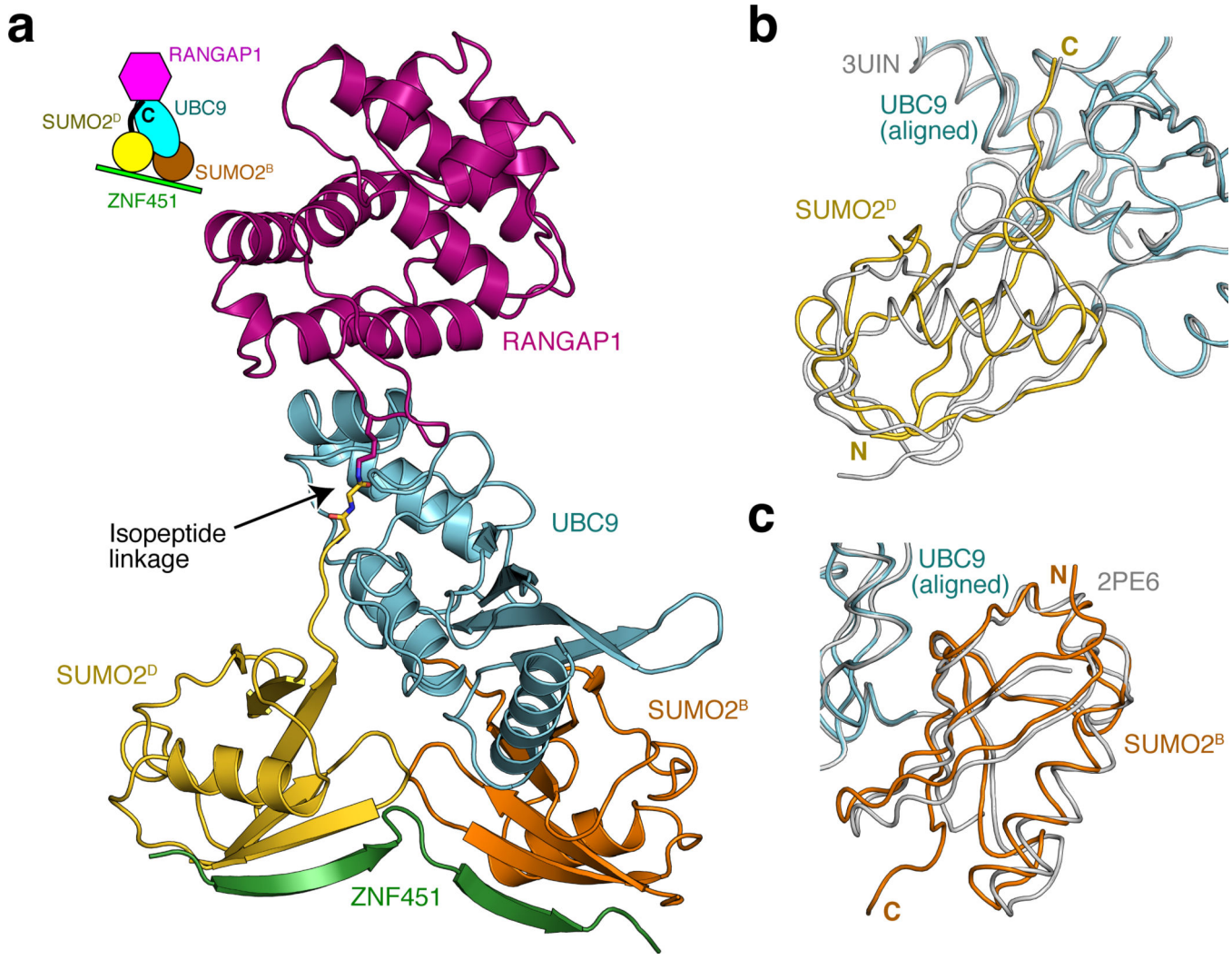

Figure 3.

Crystal structure of a ZNF451–SUMO2~RANGAP1–UBC9 complex. (**a**) Global view of the active ZNF451 complex. Top left, diagram of the complex. Bottom, active complex in cartoon representation. Only part of the asymmetric unit is represented (see Supplementary Figure 2b for the full asymmetric unit). A black arrow highlights the position of the isopeptide linkage between SUMO2 and RANGAP1. $SUMO2^{D}$ and $SUMO2^{B}$ respectively represent SUMO2 molecules in donor and backside configuration. (**b**) E2-based structural alignment between the UBC9–$SUMO2^{D}$ moiety of the ZNF451–SUMO2~RANGAP1–UBC9 complex (in colors) and the one of the RANBP2–SUMO2~RANGAP1–UBC9 complex (pdb 3UIN[13]; in gray) highlighting the similarity in the positioning of $SUMO2^{D}$ (**c**) E2–based structural alignment between the UBC9–$SUMO2^{B}$ moiety of the ZNF451–RANGAP1~SUMO2–E2 complex (in colors) and the UBC9–SUMO1 complex (pdb 2PE6[30]; in gray) highlighting the similarity in the positioning of $SUMO^{B}$.

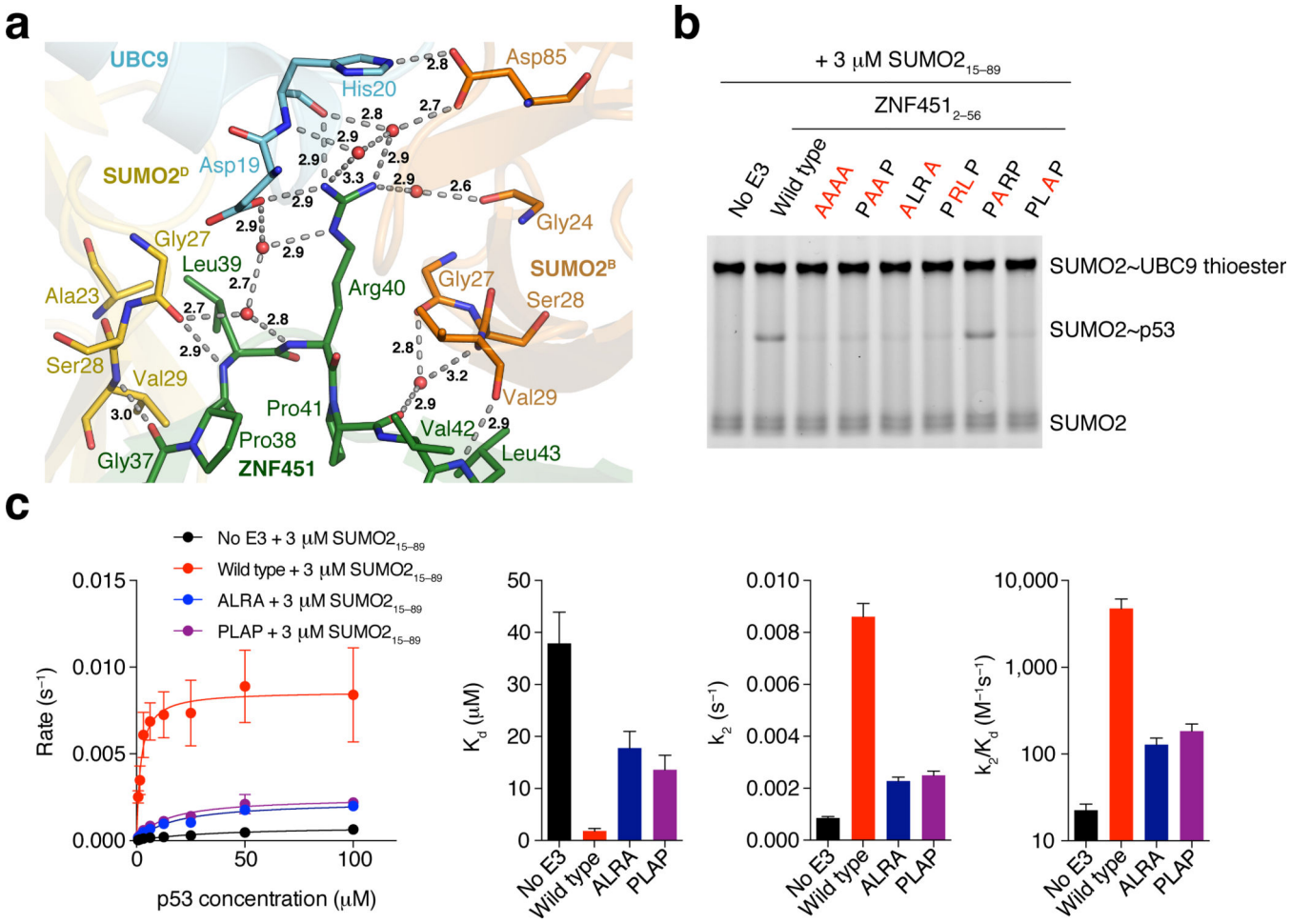

Figure 4.

The PLRP motif of ZNF451 contacts UBC9 and is important for SUMO-conjugation. (**a**) Structure of the PLRP motif of ZNF451 illustrating its interaction with UBC9, $SUMO2^D$ and $SUMO2^B$ residues. Gray dashes and bold numbers respectively represent hydrogen bonds and their length. Red spheres represent water molecules. (**b**) Single-turnover end-point assay for the conjugation of SUMO2 to the p53 tetramerization domain (residues 320–393) performed with 3 μM $SUMO2_{15–89}$ and 100 nM of $ZNF451_{2–56}$ proteins mutated to alanine at different positions in the PLRP motif. The assay was performed at 0°C for 120 seconds using 4 μM p53. Uncropped gel is shown in Supplementary Data Set 1. (**c**) Single-turnover conjugation rates of SUMO2 to p53 tetramerization domain in presence of 3 μM $SUMO2_{15–89}$ and 100 nM $ZNF451_{2–56\ ALRA}$ or $ZNF451_{2–56\ PLAP}$. Curves show mean ± s.d. (n=3 technical replicates). Representative gels are shown in Supplementary Data Set 1. Histograms are derived from the curves and present k_2, K_d and specificity (k_2/K_d) constant. Histograms show mean ± s.e.m. The histogram for the specificity constant is in logarithmic scale. Data for no E3 and wild-type $ZNF451_{2–56}$ are the same as in Figure 1b.

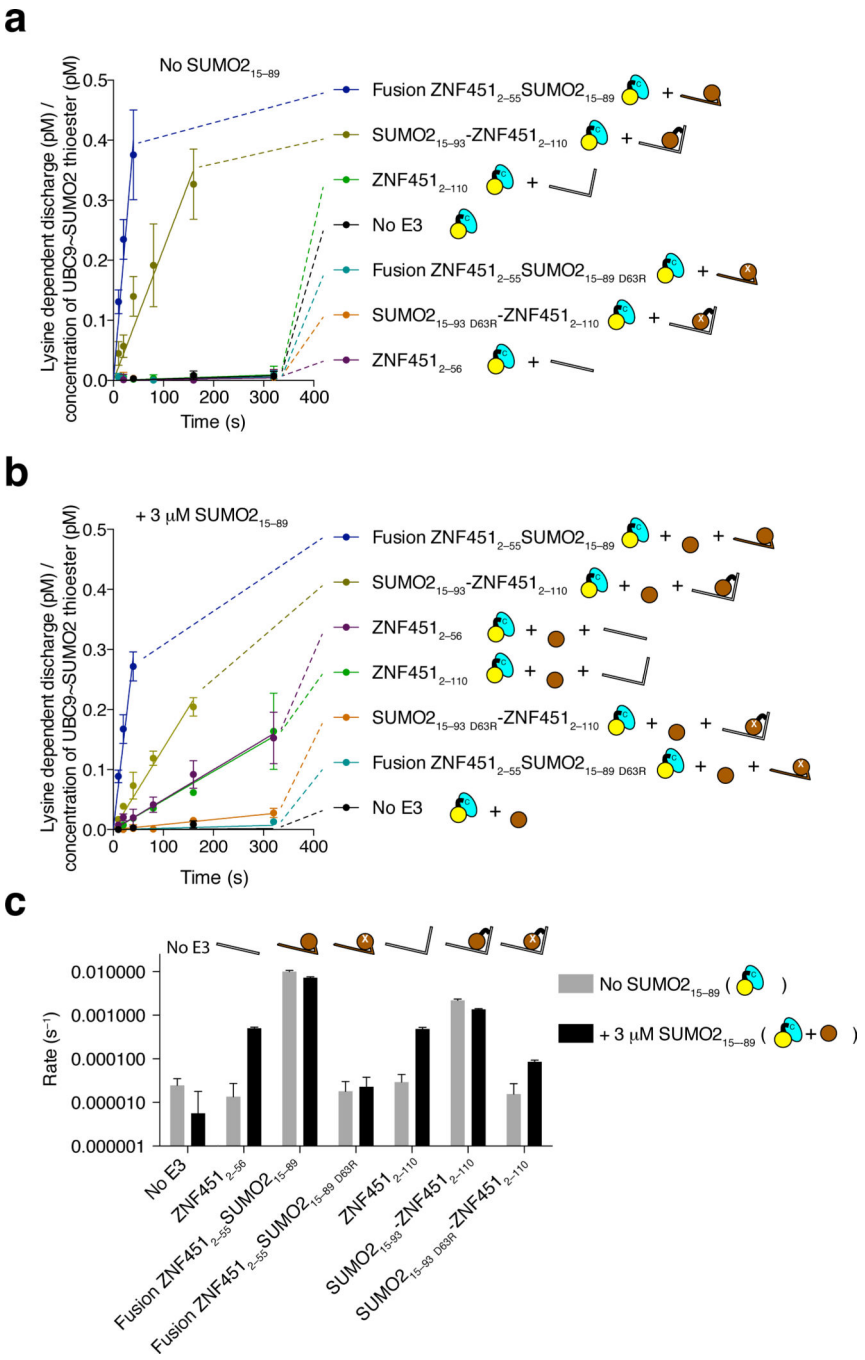

Figure 5.

SUMO2-conjugated ZNF451 or a ZNF451-SUMO2 fusion display increased SUMO2 conjugation activity. (**a, b**) Discharge assays performed using 10 mM L-lysine as a SUMO acceptor in the absence (**a**) or presence (**b**) of 3 μM $SUMO2_{15–89}$ and 100 nM of the indicated E3. Data show mean ± s.d. (n=3 technical replicates). Representative gels are shown in Supplementary Data Set 1. Lysine-dependent discharge was obtained by subtracting the concentration of discharged SUMO2 measured in absence of lysine to the concentration of discharged SUMO2 measured in presence of 10 mM L-lysine. (**c**)

Histogram in logarithmic scale showing the rate of lysine-dependent discharge in absence or presence of $SUMO2_{15–89}$ with or without 100 nM of different E3s. Data show mean ± s.e.m of experiments shown in Figures 5a and 5b.

Table 1

Data collection and refinement statistics

	Native
Data collection	
Space group	$P2_12_12_1$
Cell dimensions	
a,*b*,*c* (Å)	78.24, 115.06, 130.98
α,β,γ (°)	90, 90, 90
Resolution (Å)	46.4–2.4 (2.49–2.40) *
R_{merge}	12.0 (51.4)
$I / \sigma I$	10.9 (3.8)
Completeness (%)	99.6 (96.6)
Redundancy	7.3 (7.3)
Refinement	
Resolution (Å)	46.4–2.4 (2.49–2.40)
No. reflections	45205
R_{work} / R_{free}	19.47 / 23.44
No. atoms	
Protein	6424
Ligand/ion	20
Water	702
B-factors	
Protein	29.1
Ligand/ion	41.1
Water	29.8
R.m.s. deviations	
Bond lengths (Å)	0.003
Bond angles (°)	0.743

One crystal was used for data collection and refinement.

* Values in parentheses are for highest-resolution shell.